

# Machine Protection

*L. Fröhlich*

DESY, Hamburg, Germany

## Abstract

Conventional linacs used for modern free-electron lasers carry electron beams of unprecedented brightness with average powers ranging from a few watts to hundreds of kilowatts. Energy recovery linacs are already operated as radiation sources with nominal electron beam powers beyond 1 MW, and this figure can only be expected to increase in the future. This lecture discusses the scope of machine protection for these accelerators, reviews the parameters of existing and planned facilities, and gives an overview of typical hazards and damage scenarios. A brief introduction to the interaction of electron beams with matter is given, including a simple model for estimating some properties of electromagnetic cascades. A special problem common to most light sources—the field loss of permanent magnet undulators and its consequences for the emission of radiation—is discussed in the final section.

## Keywords

Machine protection; linear accelerators; free-electron lasers; energy recovery linacs; radiation-induced demagnetization.

## 1 Introduction

Machine protection aspects have influenced the design and operation of particle accelerators for many decades. The storage ring community has recently seen a wave of activity in this field, owing to the unprecedented amount of energy stored in the beams and in the magnets of the Large Hadron Collider. In a similar fashion, the advent of high-gain free-electron lasers (FELs) and energy recovery linacs has led to a renewed interest in high-power electron linacs as drivers of radiation sources and in the special machine protection needs of these facilities.

All of this activity has produced countless reports, conference papers, and articles concerned with specific implementations and technical details. Alas, only a few publications attempt to provide a broader view of the machine protection field; interested readers will find a selection in Refs. [1–8]. The CERN Accelerator School undoubtedly deserves credit for inspiring some of the more extensive works.

This paper does not strive for generality. Prepared for the school on FELs and energy recovery linacs, it excludes any discussion of the specific issues of hadron machines, and is instead biased towards machine protection issues for linear accelerators in light sources. The initial section tries to establish the scope of what ‘machine protection’ means for these accelerators. Afterwards, an overview of typical hazards and damage scenarios is given and the parameters of existing and planned facilities are reviewed in light of their damage potential. The central part of the paper provides a brief introduction to the interaction of electron beams with matter, which is fundamental to an understanding of many problems in the field. A discussion of the field loss of permanent magnet undulators and its consequences for the emission of radiation sheds some light on a problem specific to light sources at the end of the paper.

## 2 The scope of machine protection

The term *machine protection* is often understood as a mere synonym for a system of protective interlocks and beam loss diagnostics. While such active systems play an important role, effective protection from damage involves many fields of accelerator engineering and physics. If we attempt to define the term

in a single sentence, we might say that *machine protection is the sum of all measures that protect an accelerator and its infrastructure from the beam*. Traditionally, the focus is on the charged particle beam, but the generated photons need to be considered as well, especially in light of X-ray FELs and energy recovery linacs with unprecedented peak and average power output. If we take this definition seriously, a number of fields must be regarded as integral parts of machine protection work, or at least as closely related.

**Machine protection systems:** a machine protection system implements interlocks on components that may interfere with the safe transport of the beam (e.g., magnets, screens). It monitors the beam with instrumentation that may be generic (beam position monitors, current monitors) or specifically designed for protection purposes (beam loss monitors, dosimetry systems). When excessive beam losses or other problems are detected, the machine protection system intervenes according to a mitigation strategy—it might simply inform the operator, reduce the repetition rate, or stop the beam production.

**Collimators:** collimators and scrapers are used to limit the extent of the electron bunch (and of possible dark currents) in phase space. If there are trajectory or focusing problems, they should intercept the electron beam before it reaches sensitive components. The electromagnetic cascades originating from the interaction of high-energy electron beams with matter are not easy to contain, so care must be taken to place suitable absorbers.

**Shielding:** the loss of a small fraction of an electron beam at the gigaelectronvolt level releases a dangerous amount of spontaneous radiation. Even if the average power of the beam is as low as a few watts, the radiation can quickly cause temporary or permanent damage to electronics in the vicinity of the beamline. Sustained exposure causes various types of radiation damage—cable insulation becomes brittle, optical components darken. Beam loss can also release sizable quantities of neutrons and activate materials in the process. Depending on the beam power, accelerator components may therefore require shielding against both electromagnetic dose and neutrons.

**Beam physics:** a loss-free transport of charge from the injector to the dump requires a good understanding of the optics and of the entire acceleration process. The higher the beam power, the more important it is to have good control over the optics matching and over collective effects that create emittance blow-ups, tails, or halos.

**Robust systems:** every system or software package that has a direct or indirect influence on the beam contributes to the protection of the machine by providing a certain level of robustness. Cardinal examples are beam-based feedback systems, low-level radio-frequency systems, or even high-level physics tools for optimization of the radiation output.

**Procedures:** well-defined procedures for typical linac operations, such as switch-on, change of energy, or ramp to full power, contribute to safety and make the machine state more reproducible. Automation of these procedures can further help to avoid errors.

### 3 Beam power of existing and future facilities

When we examine the machine protection needs of an electron linac, the most important characteristic to consider is its average beam power  $P$ :

$$\begin{aligned} \text{average beam power} &= \frac{\text{energy}}{\text{charge}} \cdot \frac{\text{charge}}{\text{time}} \\ &= \frac{\text{'beam energy'}}{e} \cdot \text{average current} . \end{aligned}$$

**Table 1:** Maximum energy, bunch frequency, and average beam power of selected existing and planned FELs. The calculation of the beam power assumes typical parameters for minimum and maximum power operation for each facility.

	$E$ (GeV)	$\nu$ (Hz)	$P$ (W)
FERMI	1.4	10	14
SACLA	7	10–60	8–140
LCLS	15	120	36–360
FLASH	1.3	1M–3M pulsed	10–22k
European XFEL	17.5	4.5M pulsed	600k
LCLS-II	4	100k–1M cw	120k
NovoFEL	0.012	5.6M–22M cw	15k–60k
JLab FELs	0.2	75M cw	>1M
Future energy recovery linacs?	5	1.3G cw	500M

When the machine accelerates single bunches of charge  $Q$  at a fixed repetition rate  $\nu$ , this becomes

$$P = \frac{\nu Q E}{e},$$

where  $E$  denotes the energy per electron and  $e$  the elementary charge.

Most existing and proposed single-pass FELs are based on normal conducting linacs using S- and C-band accelerating structures. The normal conducting technology permits only a short RF pulse so that, usually, only a single bunch is accelerated per pulse. The beam power is therefore limited by the repetition rate of the RF systems, of 5–120 Hz, and by the maximum usable bunch charge, which may vary between tens of picocoulombs and a few nanocoulombs. Depending on their individual parameters, normal conducting machines transport beams from a few watts to about 400 W (the first three entries in Table 1).

Superconducting linacs can sustain the RF pulse for a considerably longer time span. This makes it possible to accelerate long bunch trains with bunch frequencies in the megahertz range, which raises the average beam power considerably. FLASH, which is still the only working single-pass FEL based on a superconducting linac, has demonstrated the transport of 1800 bunches per pulse at a bunch charge of 3 nC with a repetition rate of 5 Hz, carrying an average power of 22 kW [9]. Facilities that are already under construction have design powers in excess of 100 kW (LCLS-II, with continuous-wave RF systems) or even above 0.5 MW (European XFEL, with pulsed RF systems). It is obvious that superconducting linacs, when operated at these power levels, have a serious damage potential.

Table 1 also lists the parameters for selected energy recovery linacs—although these are oscillators instead of single-pass FELs, they are an instructive point of reference for the typical problems associated with high beam powers. The Jefferson Lab FELs, when operated with a bunch frequency of 75 MHz (continuous wave), can carry a nominal electron beam power of more than 1 MW. This means that even the loss of a tiny fraction of the electron beam can cause serious problems including mechanical damage, and, consequently, machine protection aspects are a fundamental part of the operation of the accelerator. It is a safe assumption that future superconducting single-pass FELs operating in a similar power range will share many of the problems encountered in today’s energy recovery linacs, while adding some of their own.

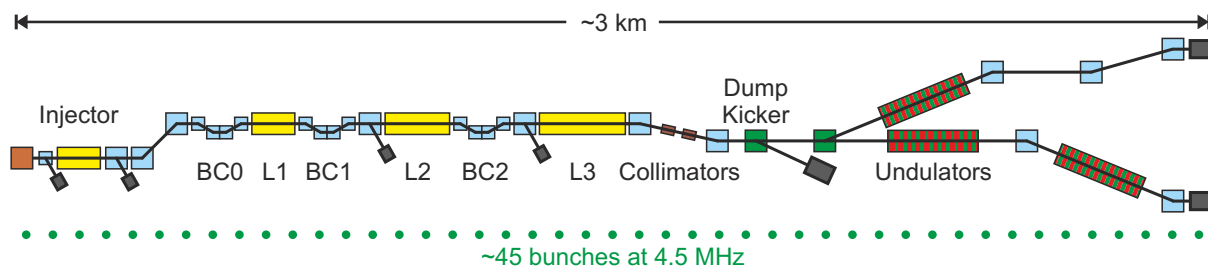


**Fig. 1:** Schematic of the European XFEL (not to scale). Main dipole magnets are shown as blue squares; accelerating sections as yellow rectangles.

#### 4 Emergency reaction times: a case study

The high repetition rates of superconducting machines bring with them some complications for the design of machine protection systems. The European XFEL (Fig. 1) is an instructive example. In the machine, the distance from the injector laser to the last undulator is approximately 3 km. Hence, a signal needs about  $10 \mu\text{s}$  to travel from one end of the accelerator to the other at the speed of light in vacuum ( $c$ ). At the maximum bunch frequency of 4.5 MHz, up to

$$3 \text{ km} \cdot 4.5 \text{ MHz}/c \approx 45$$

bunches are simultaneously travelling through the beamline. Assuming that a beam loss occurs at the farthest position from the injector and is detected immediately, the signal still needs considerable time to reach the injector laser in order to switch it off; this time would be on the order of  $15 \mu\text{s}$  for a fibre-optic transmission line with a signal propagation speed of  $\frac{2}{3}c$ . As a consequence, at least  $45 + \frac{3}{2} \cdot 45 \approx 113$  bunches would be (partially) lost before a machine protection system could take any countermeasures. At a bunch charge of 1 nC and a final energy of 17.5 GeV, these bunches would carry a total energy of

$$113 \cdot 17.5 \text{ GeV} \cdot \frac{1 \text{ nC}}{e} \approx 2 \text{ kJ},$$

enough to melt about 5 g of copper from room temperature.

In a nutshell, the efficiency of active systems for the protection of a high-power accelerator can already be limited by unavoidable signal propagation times. In such cases, greater emphasis needs to be put on passive protection measures, such as resilient and effective collimators. Sometimes it is also possible to make use of additional beam abort points—for the European XFEL, the fast dump kicker magnet can be fired when beam losses occur in the undulator sections.

#### 5 Hazards

The complete or partial loss of the electron beam in a vacuum chamber can cause a number of detrimental effects. If we try to order these effects roughly by the local power deposition needed to cause them, we obtain a list like the one in Table 2. Any such overview can only be understood as an approximate indication of the orders of magnitude; obviously, each damage scenario needs to be assessed individually and, for special cases, very different numbers may be found.

Direct mechanical damage through melting or sublimation depends on power density rather than power; for typical scenarios, however, a substantial power deposition of hundreds of watts or kilowatts is necessary—hence, direct damage is of little concern for normal conducting machines, but needs to be protected against for superconducting ones. Single-bunch damage is not to be expected for the parameters of typical FELs or energy recovery linacs because of too low charge densities; however, for the design parameters of the International Linear Collider it is a clear possibility [10].

**Table 2:** Effects of beam loss. The table roughly relates the onset of various damaging effects to the local power deposition caused by a beam loss.

$P_{\min}$ (W)	Effects
100–1000	Thermal or mechanical damage
10–100	Mechanical failure of flange connections
1–100	Activation of components
1–100	Radiation damage to electronics, optical components, etc.
1–10	Excessive cryogenic load, quenches
0.01–0.1	Demagnetization of permanent magnets

The deposition of heat can also have indirect consequences—such as impairing the tightness of a flange connection once the metal starts to cool down after thermal expansion. This, again, is an unlikely scenario for the typical beam powers of normal conducting machines, but is a real danger once the beam power reaches the multikilowatt level.

The spontaneous radiation released by beam losses can lead to malfunctions in electronics or to various types of radiation damage. In fact, the radiation released by a single watt of electron beam dumped on a beam pipe is quite destructive to many types of electronics in the vicinity if no proper shielding is in place. Such a loss is, of course, easily diagnosed in a linac operating at low current, but it only corresponds to a fraction of  $10^{-5}$  of a 100 kW beam. Similar considerations apply to the activation of components; generally, induced radioactivity at electron accelerators is relatively short-lived and substantially less than at hadron machines, but it can impair the maintainability of components and the accessibility of the beamline.

Superconducting accelerators have a special vulnerability to beam losses because any deposition of heat in the cold mass must be compensated for through the cryogenic system with a disproportionate amount of power. Beam losses can also cause superconducting cavities or magnets to quench (i.e., to become normal conducting), which in turn creates an immediate instability in the downstream beam transport. For cavities, a reduction of RF power is usually sufficient to stop a quench, whereas superconducting magnets need more intricate quench protection systems to protect them from damage.

Finally, light sources usually depend on undulators made of permanent magnets. These magnets are installed in the immediate vicinity of the beam axis and are susceptible to field loss under irradiation. This makes beam losses in insertion device sections a particular concern for machine protection. We will therefore revisit the topic in greater detail later on.

## 6 Interaction of electron beams with matter

For almost all studies related to machine protection, a good understanding of the interaction of the beam with matter is fundamental. In other words, what happens when the electrons or photons of our light source hit an obstacle?

### 6.1 How electrons lose energy

Electrons passing through matter lose kinetic energy and are deflected from their original direction. Several processes contribute to both effects, most importantly:

- elastic scattering with nuclei;
- inelastic scattering with atomic electrons;
- bremsstrahlung.

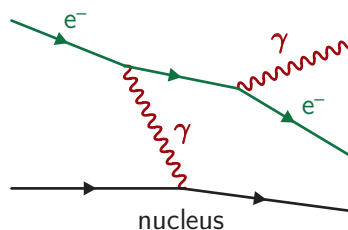


**Fig. 2:** Feynman diagram for the emission of a bremsstrahlung photon by an electron scattered at an atomic nucleus

All of these phenomena are caused by Coulomb interaction of the projectile with the atoms of the target material, but only the latter two contribute substantially to the energy loss of the electrons. In *elastic scattering* with a nucleus, the mass difference between both collision partners is so large that the electron loses only a tiny fraction of its kinetic energy. Multiple Coulomb scattering in the lattice of the target material can, however, deflect the electrons significantly from their incident direction and cause a broadening of the beam. A discussion of the angular distribution caused by multiple Coulomb scattering is found, e.g., in Ref. [11].

*Inelastic scattering* mainly takes place between the projectiles and the bound electrons of the target material. Some of the kinetic energy of the moving charge is transferred to the target atom in the form of electronic excitation or ionization. This is the only effect of any importance by which electrons can transfer energy *directly* to matter. The ESTAR online database [12] is an excellent resource for quantitative calculations and contains stopping power and range data for many materials. Readers interested in the original quantum mechanical treatment of inelastic scattering by Bethe and Bloch from the 1930s and in later corrections to the theory should consult Refs. [13–15].

*Bremsstrahlung* is the radiation emitted by fast electrons due to the interaction with the electric field of the positively charged nuclei of the target material (Fig. 2). By bremsstrahlung, the electrons lose energy without depositing it directly in matter—instead, the energy is carried away by photons, which may or may not interact with the material themselves. In the high-energy limit, these radiative losses scale almost linearly with the energy of the projectile  $E$  as

$$\frac{dE}{dx} \approx \text{const.} \cdot E \cdot \frac{Z^2}{m^2}, \quad (1)$$

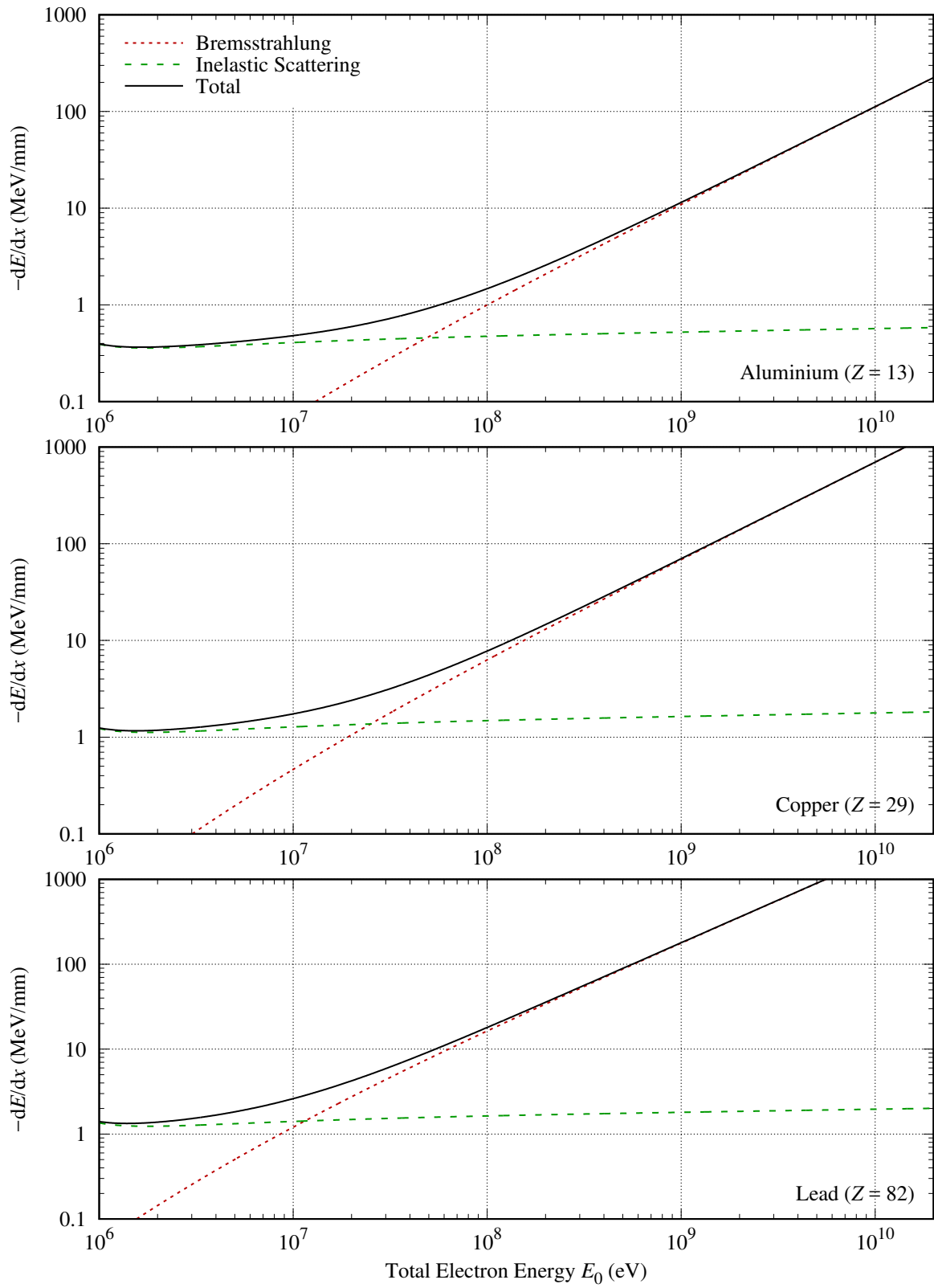
where  $dE/dx$  is the energy loss per distance travelled inside the material,  $Z$  is the atomic number, and  $m$  is the mass of the projectile. The occurrence of  $m^2$  in the denominator also indicates why bremsstrahlung is so much more important for electrons than for any other charged particles—they are light.

Figure 3 shows the contributions to the energy loss of an electron travelling through aluminium, copper, and lead. Inelastic scattering is most important at low energies, while emission of bremsstrahlung dominates the high-energy region.

For practical purposes, it is useful to know the particle energy at which the loss by inelastic scattering is equal to the radiative loss. To a good approximation, this quantity is a material constant called the *critical energy*. It can be estimated fairly well by the simple formula:

$$E_{\text{crit}} \approx \frac{800 \text{ MeV}}{Z + 1.2}.$$

Typical values are 51 MeV for aluminium, 25 MeV for copper, and 9.5 MeV for lead; more materials are listed in Ref. [16].



**Fig. 3:** Energy loss by electrons in aluminium, copper, and lead as a function of total electron energy

**Table 3:** Radiation length of selected materials [18]

Material	$L_{\text{rad}}$ (cm)	$X_0$ (g/cm <sup>2</sup> )
Aluminium	8.90	24.01
Titanium	3.56	16.16
Iron	1.76	13.84
Copper	1.43	12.86
Tungsten	0.35	6.76
Lead	0.56	6.37

## 6.2 Radiation length

As long as we are in the bremsstrahlung-dominated regime (well above the critical energy), we find that radiative losses are approximately proportional to the total energy of the electrons (Eq. (1)). Of course, this means that the energy decays exponentially with the distance  $x$  travelled in matter:

$$E(x) \approx E_0 \exp\left(-\frac{x}{L_{\text{rad}}}\right).$$

The quantity  $L_{\text{rad}}$  is a material constant called the *radiation length*. It specifies the distance after which the energy of an ultrarelativistic electron has decreased to  $1/e$  of its initial value. Some authors prefer to normalize the constant to the density  $\rho$  of the material ( $X_0 = L_{\text{rad}} \cdot \rho$ ), although the resulting quantity is no longer a *length* in the literal sense. Table 3 shows values of  $L_{\text{rad}}$  and  $X_0$  for some materials. A convenient method of calculating  $X_0$  to a precision of a few per cent is given in Ref. [17]. Using the atomic number  $Z$  and the mass number  $A$ ,

$$X_0 \approx \frac{A}{Z(Z+1) \ln(287Z^{-0.5})} \cdot 716.4 \frac{\text{g}}{\text{cm}^2}.$$

## 6.3 Interaction of photons with matter

So far, we have treated only the direct interaction of electrons with the target material. Of course, the emitted bremsstrahlung photons can interact with the material, too. The most important processes for this are:

- the photoelectric effect;
- Compton scattering;
- pair production;
- photonuclear reactions.

The first two effects lead to ionization of the material—in Compton scattering, the incident photon transfers part of its energy to an atomic electron; in the photoelectric effect it is absorbed completely—while pair production creates a positron and an electron from a photon of sufficient energy (Fig. 4). Compared with these three effects, photonuclear reactions are extremely rare. Their main importance lies in the creation of free neutrons in the giant dipole resonance, which is the main source of beam-induced activation at electron accelerators.

The interaction cross-sections of photons in aluminium, copper, and lead are shown in Fig. 5. The photoelectric effect and Compton scattering are more important at lower energies, whereas pair production is clearly the dominant process above a few tens of megaelectronvolts. As a rule of thumb, the interaction cross-section for pair production scales with the square of the atomic number,  $\sigma_{\text{pair}} \propto Z^2$ . This is essentially the same proportionality as for the energy loss of electrons due to bremsstrahlung

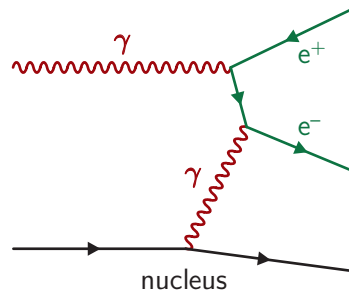


**Fig. 4:** Feynman diagram for electron–positron pair production

(Eq. (1)): unsurprisingly, heavier elements tend to provide better shielding against high-energy electron and photon beams.

In a pair production event, almost all of the photon energy is converted into the rest mass and kinetic energy of the electron–positron pair; the momentum transfer to the nucleus also participating in the interaction is negligible. Hence, the overall picture is the same as for electrons: high-energy particles do not transfer energy directly to matter; such energy absorption mainly takes place at the lower end of the energy spectrum.

A useful rule of thumb can be used to calculate the *mean free path length*  $L_{\text{pair}}$  of photons at high energies. It can be readily expressed in terms of the radiation length of the material as

$$L_{\text{pair}} \approx \frac{9}{7} L_{\text{rad}}.$$

Ignoring the difference of  $\sim 30\%$ , this translates into the following, remarkably simple result:

*The typical path length a photon can travel in matter until it is consumed in a pair production event is roughly the same as the radiation length of the material.*

On a final note, electrons and positrons are, of course, not the only particles produced in pair production events. For example, a channel for pair production of the next heavier particle, the muon, opens at photon energies of  $2m_{\text{muon}} \approx 211$  MeV. However, the cross-section for muon production is several orders of magnitude less than that for electron–positron production. While muons *can* be of concern for general radiation protection (exposure to human beings), electrons and positrons are usually the only particles produced in sufficient quantities to be considered for machine protection purposes.

#### 6.4 Electromagnetic cascades

At sufficiently high energies, the energy loss of electrons is dominated by bremsstrahlung, and the main interaction of photons with matter is the production of electron–positron pairs. Combined, these two effects create the phenomenon of an *electromagnetic cascade* or *shower*. As illustrated in Fig. 6, bremsstrahlung photons induce pair production, and the newly created electrons and positrons in turn generate bremsstrahlung when they interact with the nuclei of the material. These new photons can produce additional  $e^+/e^-$  pairs, and therefore the number of particles involved in the cascade increases exponentially until the energies are low enough to favour different processes. Hence, the effect of an electromagnetic cascade is the dispersal of transported energy from a few high-energy particles to many low-energy particles. These low-energy particles are mainly responsible for the energy transfer to the material.

#### 6.5 Simplified cascade model

It is possible to derive a coarse estimate of the penetration depth of an electromagnetic shower from a very simple model of the cascade (see, e.g., Ref. [16]). Exploiting the fact that the characteristic length

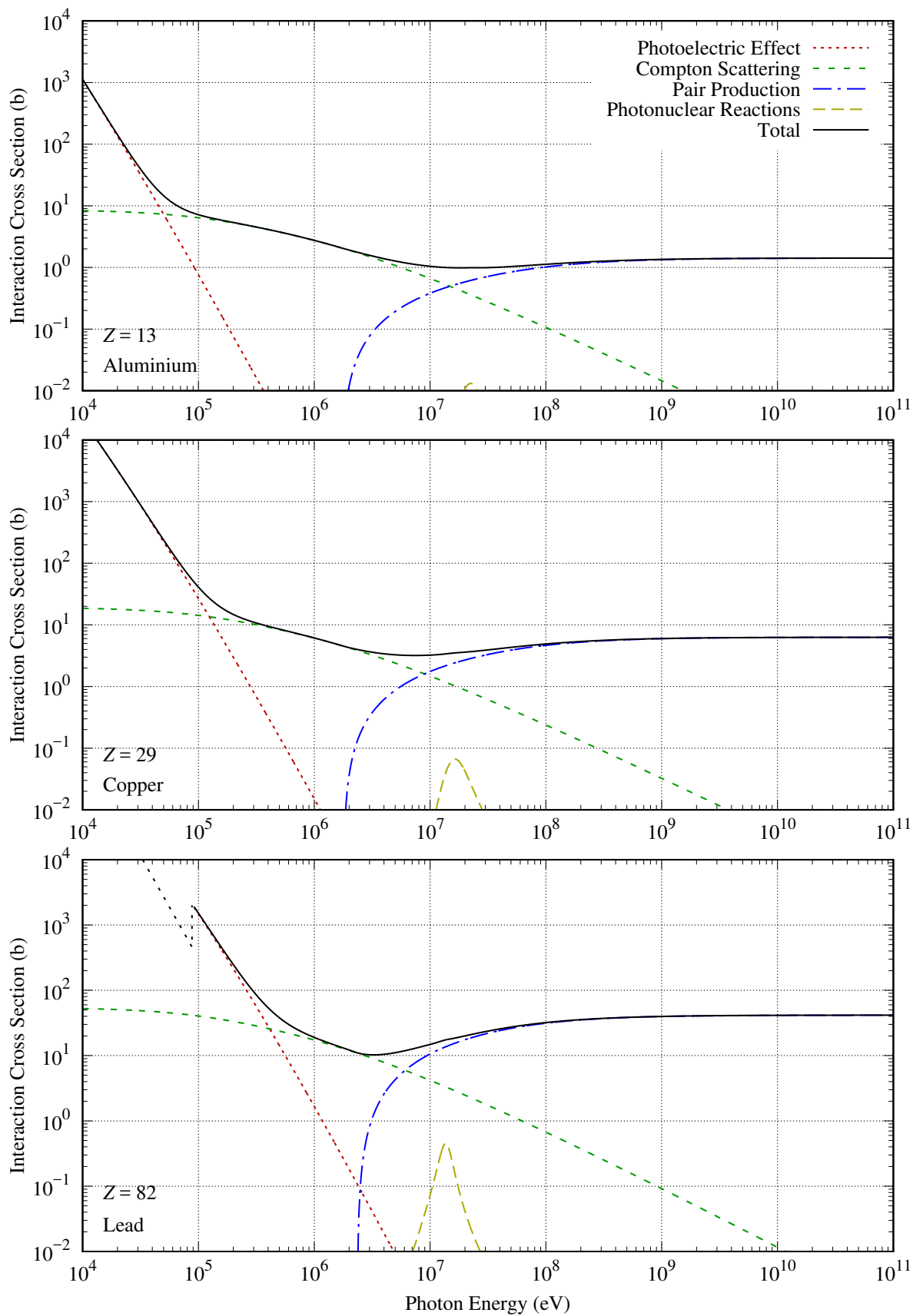


**Fig. 5:** Total cross-sections for photonic interactions in aluminium, copper, and lead

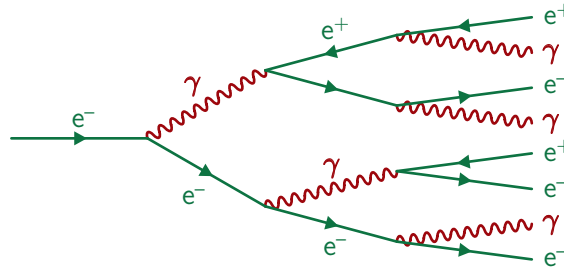


**Fig. 6:** Electromagnetic cascade as the sequence of emission of bremsstrahlung and pair production

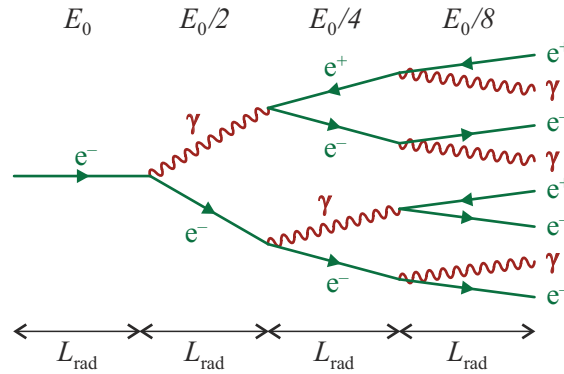


**Fig. 7:** Simplified model of electromagnetic cascade

scale of the problem is the radiation length of the material, three basic assumptions are made.

- An electron emits half of its energy as a single photon after travelling a distance  $L_{rad}$ .
- A photon is converted to an  $e^+e^-$  pair, each carrying half of its energy, after  $L_{rad}$ .
- The shower stops when particle energies drop below the critical energy.

Apart from some general approximations, these assumptions basically reduce statistical statements to deterministic rules for individual particles.

Figure 7 shows the evolution of the cascade in this simplified model. The cascade starts from a single electron of energy  $E_0$ , which emits a photon of energy  $E_0/2$  after one radiation length. More generally, after  $N$  radiation lengths, there are  $2^N$  particles, each with energy  $E_0/2^N$ .

After a certain number  $N_{crit}$  of radiation lengths, the particle energy has decreased to the critical energy of the material, and the cascade stops. From

$$E_{crit} = \frac{E_0}{2^{N_{crit}}},$$

it is straightforward to calculate the number of particle generations in the shower:

$$N_{crit} = \frac{\ln(E_0/E_{crit})}{\ln(2)}. \tag{2}$$

It is not obvious how to interpret this remarkably simple result—clearly, a real cascade does not come to a sharp stop after a certain distance. To get a feeling for the physical meaning of Eq. (2), it is instructive to calculate the values of  $N_{crit}$  for a few scenarios and to compare them against the results of more sophisticated simulations. Considering an electron beam hitting a (large) copper block, Eq. (2) yields the following values for a critical energy of  $E_{crit}(Cu) = 25$  MeV:

- for a beam energy of 100 MeV:  $N_{crit} \approx 2$ ;

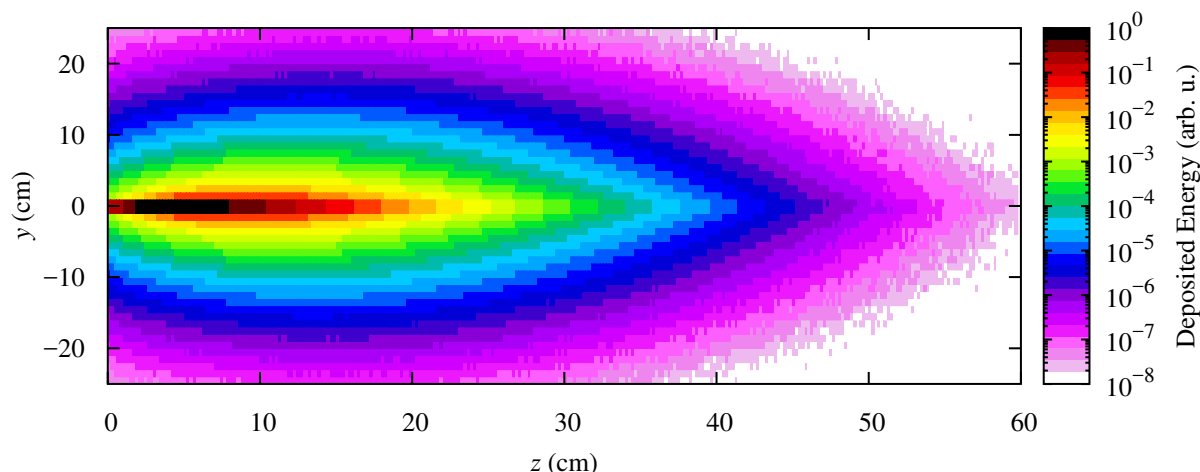


**Fig. 8:** Energy deposition by a 1 GeV pencil electron beam impinging on a big copper target. The deposited energy is averaged over the range  $-2 \text{ cm} < y < 2 \text{ cm}$ .

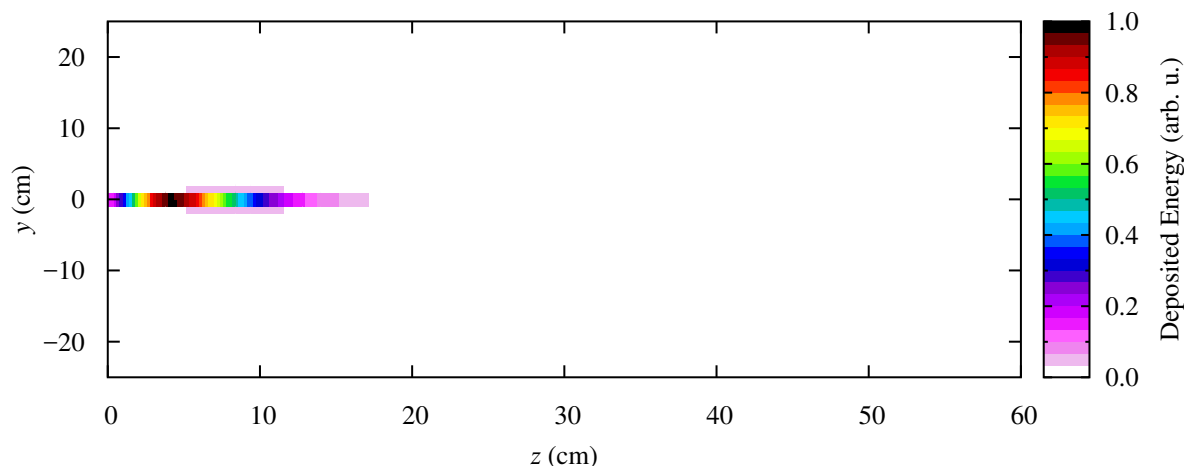


**Fig. 9:** The same plot as Fig. 8, but with a linear energy scale

- for a beam energy of 1 GeV:  $N_{\text{crit}} \approx 5.3$ ;
- for a beam energy of 10 GeV:  $N_{\text{crit}} \approx 8.6$ .

## 6.6 Monte Carlo simulations

The propagation of electromagnetic cascades in the presence of obstacles or shielding can be modelled very well by Monte Carlo simulations. In such simulations, lots of particles are tracked, and their interactions with the material are modelled by random sampling from the actual physical probability distributions. The end result of such a simulation is always obtained by averaging over the contributions of all individual particles to the quantity of interest (e.g., energy deposition or fluence). Widely used and fairly complete simulation codes—not only for electromagnetic, but also for hadronic problems—are, for instance, FLUKA [19, 20] and Geant4 [21, 22].

We can continue the discussion of the simplified shower model by comparing its results with those obtained from a simple FLUKA simulation. In this simulation, we let a (pencil) electron beam impinge on a huge target made of copper. The deposited energy in the material is scored on a Cartesian three-dimensional grid. Figure 8 shows the result for a beam energy of 1 GeV. The deposited energy is averaged over a slice of the target geometry (namely, the range with  $-2 \text{ cm} < y < 2 \text{ cm}$ ) and indicated by false colours distributed along a logarithmic scale. This kind of plot is typical for all kinds of machine

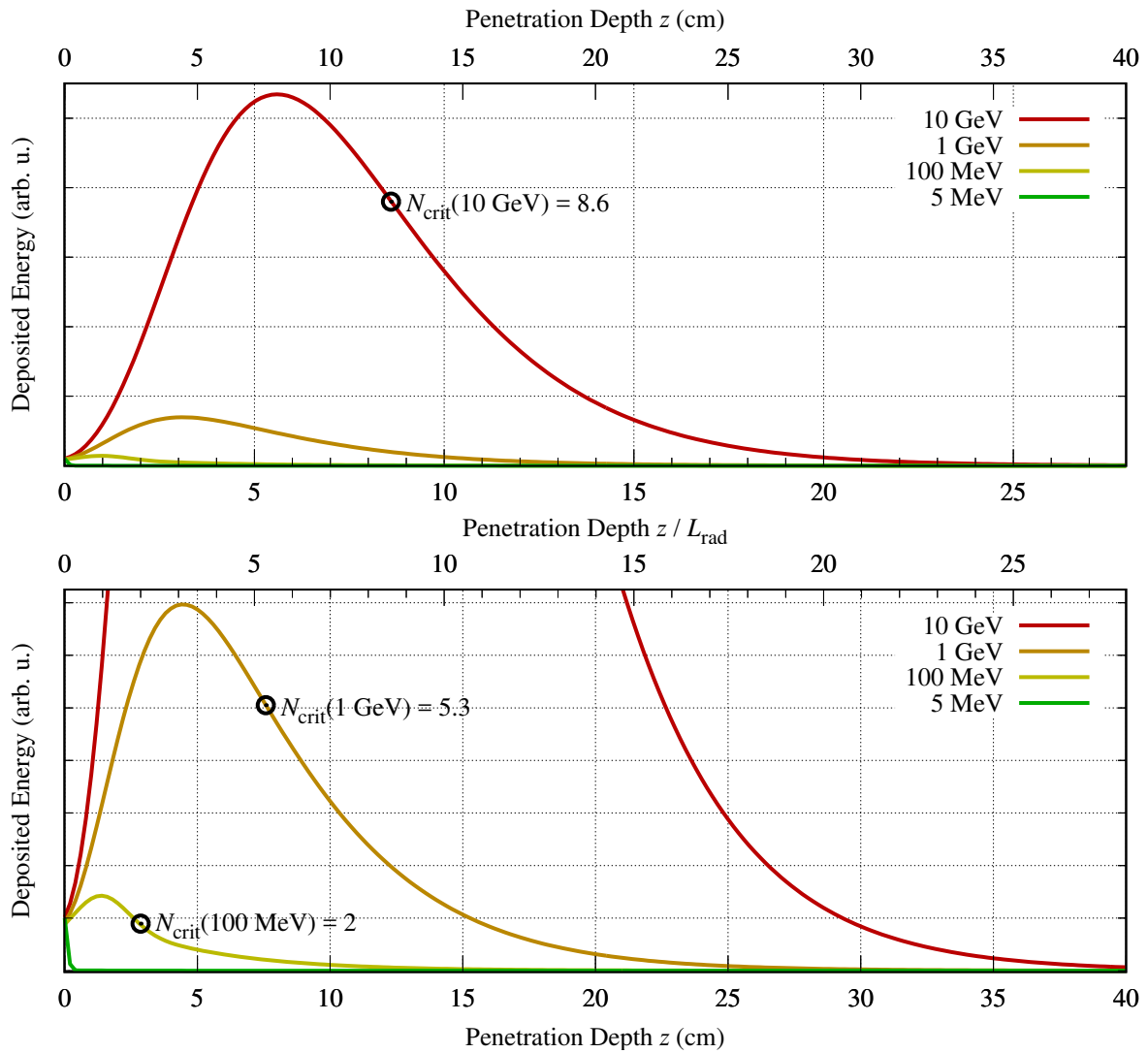


**Fig. 10:** Energy deposition by electron beams of various energies in a huge copper target. The beam impinges from the left at  $z = 0$ . Both plots show the same curves with different scales for the vertical axis.

and radiation protection studies where walls and other shielding implements attenuate radiation fields by many orders of magnitude; it can, however, be misleading because of the logarithmic colour scale. Where Fig. 8 seems to suggest that a substantial amount of energy is deposited far off-axis, the same plot with a linear energy scale (Fig. 9) shows clearly that this is not the case.

Figure 10 shows the projection of the deposited energy onto the  $z$  axis. This view is especially useful for judging the penetration depth of the shower in the material. Because the simulated copper target is huge, it absorbs all of the energy of the incoming beam. Therefore, a 10 GeV beam deposits ten times more total energy than a 1 GeV beam, which in turn deposits ten times more energy than a 100 MeV beam. All of these high-energy beams show similar curve shapes: the energy deposition rises steeply to a maximum and afterwards decreases ever more slowly, with a long tail to large penetration depths. This is simply a consequence of the statistical nature of an electromagnetic cascade: there are always some high-energy photons that traverse long stretches of the material before interacting with it. The behaviour of the electron beam at 5 MeV is different—because the beam energy is far less than the critical energy, its energy loss is dominated by inelastic electron–electron scattering, and very little bremsstrahlung is generated.

The figure also allows the results for  $N_{\text{crit}}$  from Eq. (2) to be put into context. The simple shower model reliably predicts a shower depth that is a good way beyond the actual shower maximum. For all its simplicity, the model can therefore be used for quick shielding estimates—at a thickness of about 2–3  $N_{\text{crit}}$  radiation lengths, most of the shower energy has been absorbed by the material.

## 7 Damage to permanent magnets

Free-electron lasers and energy recovery linacs used as light sources usually depend on undulators or wigglers made of permanent magnets to extract synchrotron radiation from the electron beam. Unfortunately, the beam can also damage them: permanent magnets gradually lose their magnetization under irradiation (see e.g., Refs. [23–25]). This problem is of particular concern for machine protection at light sources because:

- it is cumulative (even small beam losses or dose rates can cause a deterioration of the field over longer time-scales).
- it is often not possible, or at least very expensive, to exchange an undulator.
- the undulators represent one of the smallest apertures in the accelerator (the SACLA in-vacuum undulators have a minimum gap of 3.5 mm [26]).
- in FELs, the lasing process itself depends crucially on a high precision of the magnetic field.

As a general rule, designers of insertion devices already prefer magnetic materials of higher coercivity because they are more radiation-resistant. Nonetheless, measurements after a few years of operation in an accelerator sometimes reveal significant loss of field. For example, a sacrificial permanent magnet structure installed at FLASH lost 3% of its initial field after 3 years of operation [27], and the first period of an undulator from the Petra-II storage ring was reduced to almost half of its magnetization in the lifetime of the machine, with visible signs of demagnetization continuing at least until the 20th period of the device [28,29]. These measurements are alarming enough that we should examine the effect of a partially demagnetized undulator on the emission of synchrotron radiation in some detail.

### 7.1 Effect of demagnetization in an undulator

For a number of reasons, typical beam loss scenarios cause a very inhomogeneous dose deposition along the longitudinal axis of an undulator. The strongest demagnetization is usually to be expected in the first periods at the upstream end of the magnet structure.

To understand the effect of a partially demagnetized undulator, we can track a single electron through the centre of a perfect undulator field with a simple two-dimensional tracking code. At each turning point  $n$  of the undulating trajectory (where the transverse velocity is zero), we note the longitudinal slippage  $\Delta z_n$  between the electron and a photon emitted at the undulator entrance. In an ideal undulator, this slippage simply increases by one radiation wavelength  $\lambda_r$  for each full period of the undulating motion,  $\Delta z_{n+2} - \Delta z_n = \lambda_r$ .

If the field amplitude at the undulator entrance is reduced, the electron motion is no longer synchronous with the nominal radiation wavelength—the particle effectively takes a straighter trajectory and therefore gets ahead of where it should be. This effect can be described by a phase error  $\Delta\phi$ . At each trajectory turning point  $n$ , we define:

$$\Delta\phi_n = 2\pi \cdot \frac{n \lambda_r / 2 - \Delta z_n}{\lambda_r} + \phi_0,$$

where the starting phase  $\phi_0$  can be chosen at will (as by a phase shifter chicane in a real-world FEL).

We are going to use the parameters of an undulator in the final stage of the FEL-2 line of FERMI (Table 4) to study a real-world example. To simulate radiation-induced demagnetization, the ideal undu-

**Table 4:** Undulator and electron beam parameters for phase error calculation

Number of periods	66
Period length	3.48 cm
Field amplitude	1.105 T
Electron energy	1.25 GeV
Wavelength (fundamental)	21.7 nm

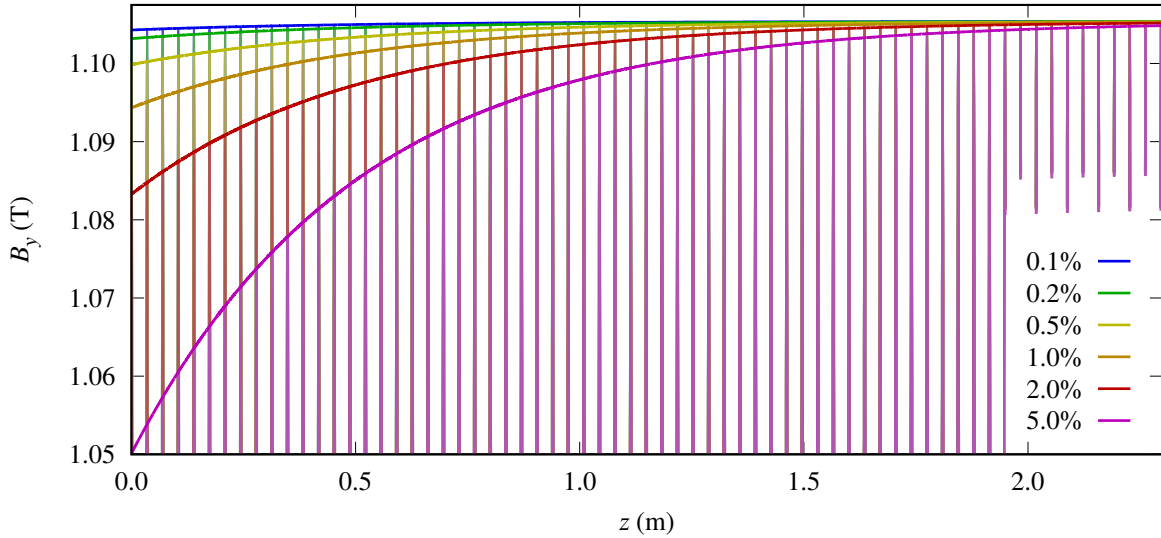


**Fig. 11:** Magnetic field profiles used for phase error calculations. Thick lines show the tapering of the field amplitude; the actual oscillating magnetic field is indicated by thinner lines below.

lator field  $B_y(z)$  is tapered exponentially according to

$$B'_y(z) = B_y(z) \cdot \left(1 - de^{(-z/L)}\right),$$

with  $L = 0.5$  m and a factor  $d$  specifying the relative demagnetization at  $z = 0$ . Field profiles for values of  $d$  between  $10^{-3}$  and  $5 \cdot 10^{-2}$  are shown in Fig. 11.

The resulting phase errors are displayed in Fig. 12. For ease of comparison, they have been adjusted (via  $\phi_0$ ) to coincide at zero at the exit of the undulator. It can be seen that the phase errors quickly reach large values: already at a tapered demagnetization of 1%, the electron bunch is out of phase by  $90^\circ$  at the undulator entrance. For higher values of  $d$ , the electron bunch in the first part of the structure effectively cancels out a part of the radiation through destructive interference. It should be noted that inhomogeneous phase errors like this can only partially be compensated by adjusting the undulator gap—after all, opening the undulator gap is equivalent to the introduction of a linear phase slope.

Obviously, the effect on the microbunching and on the final output power of an FEL needs to be studied in the context of the whole system of insertion devices and electron beam optics. It is clear, however, that even a small loss of magnetic field can have a big influence on the performance of an undulator.

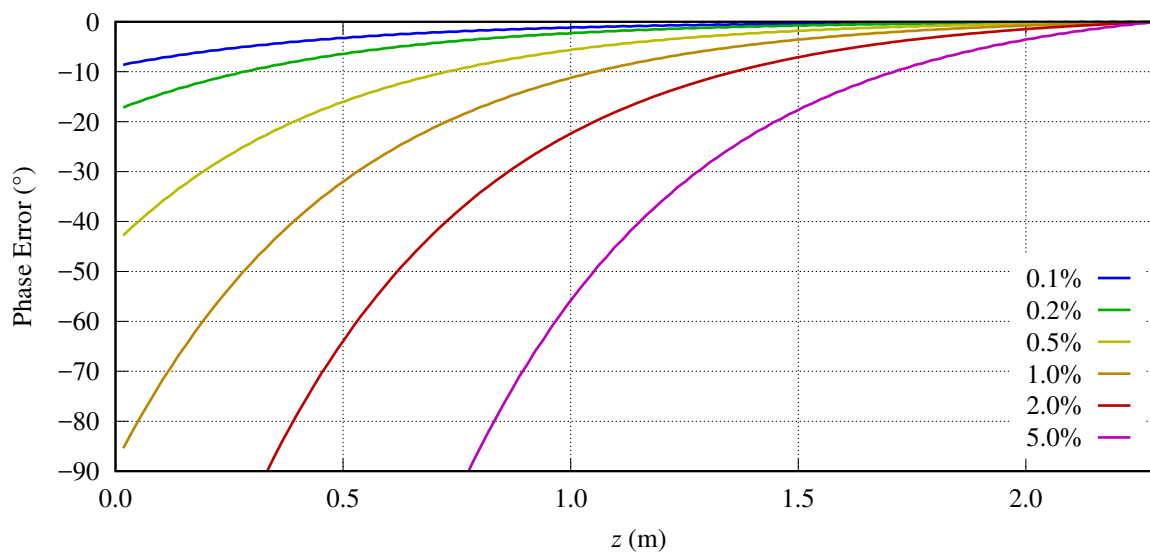


**Fig. 12:** Resulting phase errors for various demagnetization profiles. The reference point for all phases is the exit of the undulator.

## 8 Conclusions

All synchrotron light sources share a common set of machine protection problems: the limitation of induced activation, the protection of components from radiation damage, and the protection of permanent magnet undulators from demagnetization. The latter is of particular concern for FELs because magnet damage can directly impair the FEL process itself. The high beam power of superconducting or energy recovery linacs makes all of these problems much more challenging and adds the potential for direct or indirect mechanical damage. In this context, it is quite natural to see catastrophic, sustained losses of the entire beam as the main danger in high-powered accelerators. However, while such an incident can obviously have dramatic consequences, it is also relatively easy to detect and to avoid. The more serious problem with powerful beams is that even tiny fractional losses can represent huge absolute power depositions: a loss of  $10^{-4}$  of a 1 MW beam is not easily measurable by beam current monitors, but it still represents 100 W of power. To control beam losses to this level, possible causes have to be understood and many aspects of the accelerator operation have to be optimized. Ultimately, the goal of machine protection is to avoid damage to expensive components and to prevent the loss of beam time—one of the most precious resources at any light source. The best approach to this goal is not to reduce machine protection to a mere system of interlocks, but to make safety considerations an integral part of the design and operation of an accelerator.

## References

- [1] C. Sibley, Machine protection strategies for high power accelerators, Proc. PAC'03, Portland, USA, 2003 (IEEE, New York, 2003), p. 607, <http://doi.org/10.1109/pac.2003.1288989>.
- [2] R. Schmidt *et al.*, *New J. Phys.* **8** (2006) 290, <http://doi.org/10.1088/1367-2630/8/11/290>.
- [3] K. Wittenburg, in Proc. CERN Accelerator School on Beam Diagnostics, Dourdan, France, 28 May–6 June 2008, edited by D. Brandt (CERN, Geneva, 2009), p. 249, <http://doi.org/10.5170/CERN-2009-005.249>
- [4] L. Fröhlich, Machine protection for FLASH and the European XFEL, Ph.D. thesis, Hamburg University, 2009, <http://doi.org/10.3204/DESY-THESIS-2009-012>.
- [5] L. Fröhlich, Machine protection for single-pass FELs, Proc. FEL'12, Nara, Japan, 2012 (JACoW, Geneva, 2012), p. 345.

- [6] R. Schmidt, in Proc. CERN Accelerator School on Advanced Accelerator Physics, Trondheim, Norway, 18–29 August 2013, edited by W. Herr (CERN, Geneva, 2014), p. 221, <http://dx.doi.org/10.5170/CERN-2014-009.221>
- [7] J. Wenninger, State-of-the-art and future challenges for machine protection systems, Proc. IPAC'14, Dresden, Germany, 2014 (JACoW, Geneva, 2014), p. 4060.
- [8] I. Strašik, Machine protection, CERN Accelerator School: Introduction to Accelerator Physics, Prague, Czech Republic, 2014, <http://cas.web.cern.ch/cas/CzechRepublic2014/Lectures/Strasik.pdf>.
- [9] N. Walker *et al.*, Operation of the FLASH linac with long bunch trains and high average current, Proc. PAC'09, Vancouver, Canada, 2009 (JACoW, Geneva, 2009), p. 2766.
- [10] *The International Linear Collider technical design report vol. 3.II: Accelerator baseline design*, edited by C. Adolphsen *et al.*, 2013, <http://www.linearcollider.org/ILC/Publications/Technical-Design-Report>.
- [11] G.R. Lynch and O.I. Dahl, *Nucl. Instrum. Methods Phys. Res. B* **58** (1991) 6, [http://doi.org/10.1016/0168-583X\(91\)95671-Y](http://doi.org/10.1016/0168-583X(91)95671-Y).
- [12] M.J. Berger *et al.*, Stopping-power & range tables for electrons, protons, and helium ions, NISTIR 4999, National Institute of Standards and Technology, 2005, <http://www.nist.gov/pml/stopping-power-range-tables-electrons-protons-and-helium-ions>.
- [13] H. Bethe, *Ann. Phys.* **397** (1930) 325, <http://doi.org/10.1002/andp.19303970303>.
- [14] F. Bloch, *Ann. Phys.* **408** (1933) 285, <http://doi.org/10.1002/andp.19334080303>.
- [15] S.M. Seltzer and M.J. Berger, *Int. J. Appl. Radiat. Isot.* **35** (1984) 665, [http://doi.org/10.1016/0020-708X\(84\)90113-3](http://doi.org/10.1016/0020-708X(84)90113-3).
- [16] W.R. Leo, *Techniques for Nuclear and Particle Physics Experiments: A How-To Approach* (Springer, Berlin, 1994), <http://doi.org/10.1007/978-3-642-57920-2>.
- [17] W.-M. Yao *et al.* (Particle Data Group), *J. Phys. G* **33** (2006) 1, <http://doi.org/10.1088/0954-3899/33/1/001>.
- [18] K.A. Olive *et al.* (Particle Data Group), *Chin. Phys. C* **38** (2014) 090001, <http://doi.org/10.1088/1674-1137/38/9/090001>.
- [19] T.T. Böhlen *et al.*, *Nucl. Data Sheets* **120** (2014) 211, <http://doi.org/10.1016/j.nds.2014.07.049>.
- [20] A. Ferrari *et al.*, FLUKA: a multi-particle transport code, CERN-2005-10 (2005), INFN/TC\_05/11, SLAC-R-773.
- [21] S. Agostinelli *et al.*, *Nucl. Instrum. Methods A* **506** (2003) 250, [http://doi.org/10.1016/S0168-9002\(03\)01368-8](http://doi.org/10.1016/S0168-9002(03)01368-8).
- [22] J. Allison *et al.*, *IEEE Trans. Nucl. Sci.* **53** (2006) 270, <http://doi.org/10.1109/TNS.2006.869826>.
- [23] A.B. Temnykh, *Nucl. Instrum. Methods A* **587** (2008) 13, <http://doi.org/10.1016/j.nima.2008.01.002>.
- [24] Y. Asano *et al.*, *J. Synchrotron Radiat.* **16** (2009) 317, <http://doi.org/10.1107/S0909049509008899>.
- [25] T. Bizen, Brief review of the approaches to elucidate the mechanism of the radiation-induced demagnetization, ERL Workshop 2011, Tsukuba, Japan.
- [26] C. Pellegrini, The challenge of 4th generation light sources, Proc. IPAC'11, San Sebastián, Spain, 2011 (JACoW, Geneva, 2011), p. 3798.
- [27] J. Skupin *et al.*, Undulator demagnetization due to radiation losses at FLASH, Proc. EPAC'08, Genoa, Italy, 2008 (JACoW, Geneva, 2008), p. 2308.
- [28] H. Delsim-Hashemi *et al.*, Status of the sFLASH undulator system, Proc. FEL'09, Liverpool, UK, 2009 (JACoW, Geneva, 2009), p. 500.
- [29] P.V. Vagin *et al.*, *J. Surf. Invest.* **5** (2011) 1055, <http://doi.org/10.1134/S1027451011110218>.